ChemPubSoc Europe

DOI: 10.1002/chem.201501866

CHEMISTRY A European Journal Full Paper

Magnetic Materials

Tuning the Magnetic Interactions and Relaxation Dynamics of Dy_2 Single-Molecule Magnets

Shufang Xue,[a] Yun-Nan Guo,[c] Liviu Ungur,*[b] Jinkui Tang,*[a] and Liviu F. Chibotaru[b]

Abstract: Efficient modulation of single-molecule magnet (SMM) behavior was realized by deliberate structural modification of the Dy_2 cores of $[Dy_2(\mathbf{a'povh})_2(OAc)_2(DMF)_2]$ (**1**) and $[Zn_2Dy_2(\mathbf{a'povh})_2(OAc)_6]\cdot 4H_2O$ (**2**; $H_2\mathbf{a'povh} = N'$-[amino(pyrimidin-2-yl)methylene]-*o*-vanilloyl hydrazine). Compound **1** having fourfold linkage between the two dysprosium ions shows high-performance SMM behavior with a thermal energy barrier of 322.1 K, whereas only slow relaxation is observed for compound **2** with only twofold connection between the dysprosium ions. This remarkable discrepancy is mainly because of strong axiality in **1** due to one pronounced covalent bond, as revealed by experimental and theoretical investigations. The significant antiferromagnetic interaction derived from bis(μ_2-O) and two acetate bridging groups was found to be crucial in leading to a nonmagnetic ground state in **1**, by suppressing zero-field quantum tunneling of magnetization.

Introduction

Lanthanide single-molecule magnets (SMMs) with fascinating physical properties have attracted considerable interest in applications such as quantum information processing,[1] molecular spin valves,[2] and transistors.[3] A basic effect exploited in these envisioned applications is the property of molecule whereby the ground electronic multiplet of the spin carrier provides a strong axial anisotropy and is largely separated from the less anisotropic excited multiplets.[4] With these two underlying prerequisites, the magnetic moment of the individual molecule is blocked along the easy axis for a long time, and then each molecule behaves as a tiny magnet. The SMM behavior observable in lanthanide-containing molecules is due to an inherently unparalleled anisotropy caused by spin–orbit coupling and crystal-field effects. Recently, research on lanthanide SMMs has yielded a flood of groundbreaking results[5] including new records for the relaxation energy barrier and the blocking temperature[6] and magnetic memory in single-molecule toroics[7] after the seminal reports of Ishikawa et al. on a terbium phthalocyaninate[8] and Powell et al. on a noncollinear dysprosium triangle.[9]

However, a major drawback in such systems is fast zero-field quantum tunneling of magnetization (QTM), which prevents the isolation of high-performance lanthanide SMMs with high barrier and high hysteresis temperature. Numerous experimental and theoretical studies have demonstrated that one way to address this challenge is to design a high degree of axiality of the ligand field.[4b,10] One efficient chemical route for guaranteeing an axial ligand field is to employ highly symmetrical ligands without bonding atoms on the symmetry axis.[4b] Two typical examples of such a paradigm shift are provide by $Tb(Pc)_2^-$[8] and $[Er(COT)_2]^-$[11] SMMs, in which the metal center is sandwiched between two coplanar ligands in D_{4d} or D_{8h} symmetry. Another way is to have only one pronounced chemical covalent bond in a molecule.[12] Such a strong covalent interaction leads to an intrinsically axial nature of the total ligand field felt by the metal ion, and thus offers a new paradigm for single-ion anisotropy, as predicted for the $[DyO]^+$ cation[12] and verified in the case of individual Dy ions in mononuclear,[13] dinuclear,[14] and tetranuclear[15] dysprosium SMMs. On the other hand, more recently the role of magnetic interaction between two spin carriers has become of major importance in suppressing quantum tunneling at low temperatures.[16] Due to the core nature of the 4f orbitals, to date only some diffusing donor bridges (e.g., S[17] and radical[6,16,18]) have shown the potential to prompt magnetic interactions between lanthanide centers. In particular, Long and co-workers constructed the strongest magnetically coupled Tb_2 SMMs through an N_2^{3-} radical bridge with magnetic hysteresis up to 14 K,[6] and thus pushed the capacity of SMMs towards more practical use. In this regard, dinuclear lanthanide complexes, as opposed to other systems, provide ideal models to map the synergic effect between single-ion anisotropy and magnetic interactions in enhancing the anisotropic barrier. From the standpoint of magnetostructural correlations, such synergic effects can be in-

[a] *S. Xue, Prof. Dr. J. Tang*
State Key Laboratory of Rare Earth Resource Utilization
Changchun Institute of Applied Chemistry
Chinese Academy of Sciences, Changchun 130022 (P.R. China)
E-mail: tang@ciac.ac.cn

[b] *Dr. L. Ungur, Prof. Dr. L. F. Chibotaru*
Theory of Nanomaterials Group and
INPAC Institute for Nanoscale Physics and Chemistry
Katholieke Universiteit Leuven, Celestijnenlaan, 200F, 3001 (Belgium)

[c] *Dr. Y.-N. Guo*
School of Science, Xi'an Jiaotong University, Xi'an, 710049 (P.R. China)

Supporting information for this article is available on the WWW under http://dx.doi.org/10.1002/chem.201501866.

fluenced by the molecular symmetry,[19] the coordination environment,[20] the electronegativity of the targeted ligand,[21] and the type of bridging groups.[6,14,16–18,22]

With this in mind, we performed a thorough analysis of magnetic relaxation for two magnetically interesting dinuclear dysprosium complexes $[Dy_2(\mathbf{a'povh})_2(OAc)_2(DMF)_2]$ (**1**) and $[Zn_2Dy_2(\mathbf{a'povh})_2(OAc)_6]\cdot 4H_2O$ (**2**), with the aim of shedding light on slow magnetic relaxation and quantum tunneling effects influenced by the above-mentioned synergic effect. Magnetic anisotropy and interaction of dysprosium(III) cations could be modified by incorporating two Zn^{II} ions in the pockets on either side of the Dy_2O_2 core. Ab initio calculations revealed that **1** has very high axial magnetic anisotropy owing to pronounced coordination of one atom and stronger antiferromagnetic interaction due to four exchange paths, and thus shows better SMM behavior than the less axial **2**.

Results and Discussion

Our work has concentrated on *o*-vanilloyl hydrazone ligand *N*′-[amino(pyrimidin-2-yl)methylene]-*o*-vanilloyl hydrazine (H_2**a′povh**), which is versatile in terms of denticity and tautomerism. Recent work has revealed that complexation of H_2**a′povh** with Dy^{III} ions strongly depends on the counterion, and $[Dy_4]$[23] and $[Dy_2]_2$[24] molecules are generated when noncoordinating perchlorate and monodentate carboxyl groups are introduced, respectively. From the structural point of view, it was expected that a solvent with versatile coordination ability would influence the structural diversity of the products. The reaction of H_2**a′povh** with dysprosium acetate in methanol/DMF led to the formation of centrosymmetric dinuclear compound $[Dy_2(\mathbf{a'povh})_2(OAc)_2(DMF)_2]$ (**1**). In this case, the H_2**a′povh** ligand coordinates to two Dy^{III} ions with the tridentate N_2O pocket and bidentate *o*-vanilloyl group, and thus the Dy^{III} ions have an N_2O_6 coordination sphere (Figure 1 and Figure S1 of the Supporting Information). To probe the effect of coordination environment on the magnetic memory effect, we introduced diamagnetic zinc(II) ions to preferentially occupy the N_2O pocket and thus leave two potentially bidentate O_2 pockets vacant. The reaction of $Zn(OAc)_2\cdot 2H_2O$ and $Dy(OAc)_3\cdot H_2O$ with H_2**a′povh** produced heterometallic compound $[Zn_2Dy_2(\mathbf{a'povh})_2(OAc)_6]\cdot 4H_2O$ (**2**), in which the tridentate N_2O pocket is occupied by a Zn^{II} ion and thus a purely oxygen ligated coordination sphere is generated for the Dy^{III} center (Figure 1 and Figure S1 of the Supporting Information). Details of the structure solution and refinement are summarized in Table S1 of the Supporting Information, and selected bond lengths and angles are listed in Table S2.

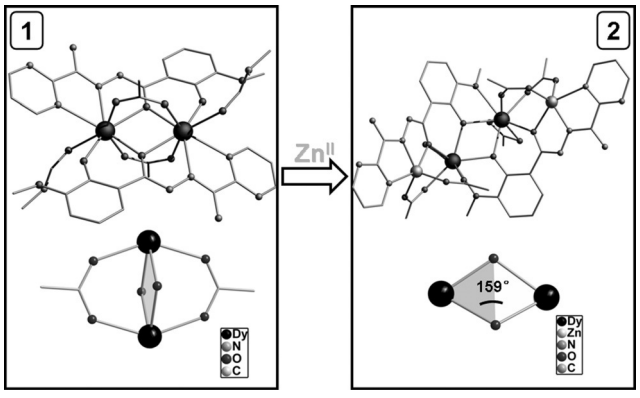

Figure 1. A perspective view of the molecular and core structures of **1** and **2**. Hydrogen atoms have been omitted for clarity.

A structural study on **1** showed it to be a centrosymmetric dinuclear dysprosium complex crystallizing in triclinic space group $P\bar{1}$ (Figure 1 and Figure S1 of the Supporting Information). The asymmetric unit contains one Dy^{III} ion, one $\mathbf{a'povh}^{2-}$ ligand, one acetate ion, and one DMF molecule, which lies on an inversion center, and no solvent molecules of crystallization were found in the lattice. Each fully deprotonated ligand coordinates to two Dy^{III} ions in a μ_2-η^1:η^1:η^2:η^1 coordination mode through the tridentate unit (N1, N4, and O1) and the bidentate *o*-vanilloyl group (O1 and O2). Carbonyl oxygen atoms (O1 and O1*) of the ligands bridge two metal centers in the conjugate deprotonated enol form (O^-), giving rise to a four-membered planar Dy_2O_2 core with a Dy1-O1-Dy1* angle of 102.62(13)° and Dy–O distances of 2.397(4) and 2.313(4) Å. Furthermore, two acetate ions straddle two Dy^{III} ions in a *syn-syn* μ_2-η^1:η^1 fashion affording a shorter Dy···Dy separation of 3.6768(5) Å compared to other centrosymmetric Dy_2 complexes.[14a,25] The required coordination pocket is occupied by one DMF molecule, and hence the Dy^{III} ion exhibits a nonsymmetric N_2O_6 coordination environment with a hula-hoop-like geometry, in which the cyclic ring (hula hoop) is defined by the atoms O1, O1*, O5, N1*, and N4*. Close inspection of the covalent bonds between the metal center and the coordinated atoms reveals that the coordinative covalent interaction with the terminal phenoxo groups (O2 and its equivalent O2*) is strongest with a Dy–O2 distance of 2.193(4) Å, which favors an axial nature of the ligand field and thus influences the single-ion anisotropy (see below).

Compound **2** crystallizes in the monoclinic space group *C*2/*c*, and consequently the whole molecule exhibits C_2 crystallographic symmetry. The asymmetric unit of **2** (Figure 1 and Figure S1 of the Supporting Information) consists of a $[Zn(\mathbf{a'povh}^{2-})Dy(OAc)]^{2+}$ dinuclear cation connected by two acetate ions in a *syn-syn* μ_2-η^1:η^1 mode. As expected, each ligand coordinates to three metal centers (Dy1, its equivalent, Dy1*, and Zn1) through the compartmentally addressable sites: the softer nitrogen atoms (N1 and N4) are bound to the Zn^{II} ion, and the *o*-vanilloyl group is occupied by Dy1 and its equivalent Dy1* according to the geometrical coordination preference of the metal centers. Dy1 and Zn1 are bridged by two deprotonated enol-form (O^-) groups with a Dy···Zn separation of 3.6555(16) Å. The central Dy^{III} ions bridged by two phenoxido groups (O2 and O2*) form a Dy_2O_2 core with a dihedral angle of 159° and Dy···Dy separation of 3.7613(13) Å, which is slightly longer than that in **1**. In contrast to **1**, Dy1 in **2** has a relatively symmetric O_8 coordination sphere derived from one enol-formal carbonyl atom (O1), one methoxide group (O3), two phenoxo atoms (O2 and O2*) from the ligands and two acetate ions (O5 and O7) in a *syn-syn* μ_2-η^1:η^1 mode, and one ace-

tate ion (O8 and O9) in η^2 fashion. The Dy–O distances range from 2.284(4) to 2.504(5) Å. Regarding the coordination geometry, the eight-coordinate Dy1 center exhibits a similar hula-hoop-like geometry, and the five-coordinate Zn^{II} ion is located in a typical tetragonal-pyramidal coordination environment.

The distances between nearest-neighbor molecules are about 7.432(4) and 9.5355(11) Å for **1** and **2**, respectively, because of different intermolecular hydrogen-bonding acceptors (Supporting Information, Figure S2).

Magnetic properties

Temperature-dependent dc susceptibilities of **1** and **2** were measured at 1000 Oe (Figure 2). The room-temperature $\chi_M T$ products for **1** and **2** (ca. 27.27 and 26.05 $cm^3 K mol^{-1}$, respectively) are nearly in consistent with the expected value

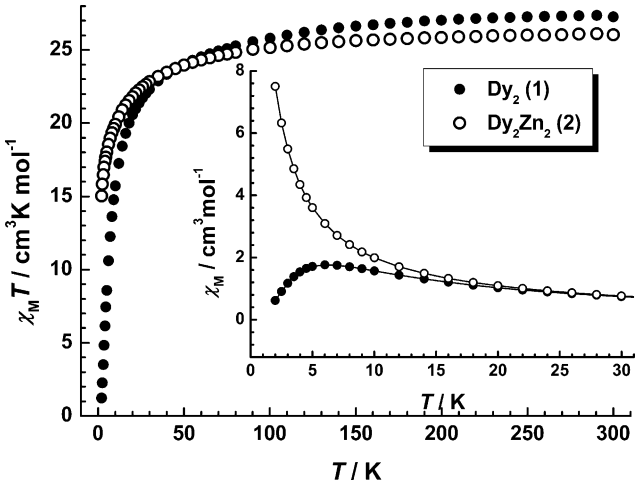

Figure 2. Temperature dependence of $\chi_M T$ products at 1000 Oe for **1** (full) and **2** (empty). Inset: temperature dependence of the magnetic susceptibility for **1** and **2** at low temperatures.

(28.34 $cm^3 K mol^{-1}$) for the $^6H_{15/2}$ state.[26] As the temperature is lowered, the $\chi_M T$ values decrease at a steady rate (300–50 K) before a more pronounced decrease occurs below 50 K, at which point the two compounds display dramatically different thermal behaviors. The observed thermal evolution below 50 K in the $\chi_M T$ plot of **1** decreases faster than that of **2** down to the corresponding minima of 1.23 and 15.03 $cm^3 K mol^{-1}$ at 1.9 K (Figure 2). The decrease in $\chi_M T$ in both cases is attributed to the depopulation of the m_J sublevels of the ground-state multiplet, with the possibility of weak antiferromagnetic interactions. Interestingly, for **1**, the maximum observed around $T=$ 6 K in the low-temperature range of the $\chi_M(T)$ plot gradually disappears with increasing dc field, suggestive of the presence of weak antiferromagnetic interactions (Figure 2, inset and Figure S3 of the Supporting Information), whereas the dominant interaction is negligibly weak in **2**, as no maximum was observed in the $\chi_M(T)$ plot (Figure 2, inset).

The magnetization data, plotted as M versus H, are shown in Figure S4 (Supporting Information). For **1**, the variable-field magnetization at 1.9 K shows an unusual inflection around 0.6 T and then increases abruptly up to the saturated value of 13.04 μ_B at 7 T. Such a peculiar well-defined step has been observed in noncollinear magnetic molecules.[9,27] The magnetization in **2** merely displays a monotonic increase with H at low fields to the "saturated" value of 11.37 μ_B at 2 K and 7 T.

The ac magnetic susceptibility data collected for both compounds under zero applied dc field display out-of-phase susceptibility (χ'') signals with frequency and temperature dependence indicative of slow relaxation that is typical for SMM behavior (Figure 3 and Figures S5–S8 of the Supporting Information). For **1**, χ'' shows a frequency-dependent full peak with maximum at temperatures as high as 30 K (for $\nu=1500$ Hz) and at frequencies as low as 0.1 Hz (at $T=1.9$ K), which indicates freezing of spins by a rather high thermal energy barrier to relaxation and the efficient suppression of zero-field tunneling of magnetization in this complex. The single relaxation mode in the frequency-dependent ac susceptibility is ascribed to the presence of only one crystallographically independent Dy^{III} ion in the centrosymmetric complexes. Fitting the thermally induced relaxation data at temperatures ranging from 24 to 30 K to the Arrhenius law (Figure 4) afforded a significantly high effective barrier to magnetization reversal: $U_{eff}=322.1$ K with $\tau_0=3.4\times10^{-9}$ s, in accordance with the energy of the first excited state (219.6 cm^{-1}) determined by ab initio calculations (see below). The thermally activated barrier is the largest yet among reported antiferromagnetically coupled dinuclear sys-

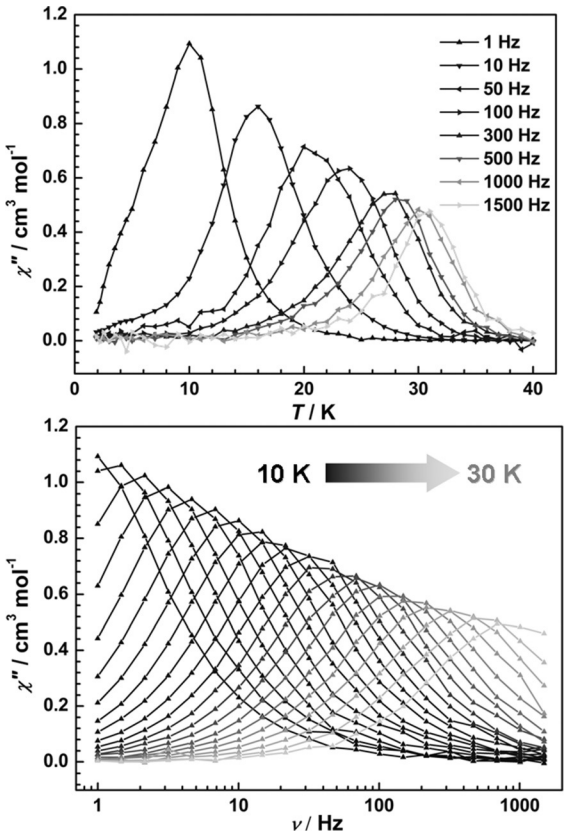

Figure 3. Temperature and frequency dependence of the out-of-phase (χ'') part of the ac susceptibility for **1** in zero dc field.

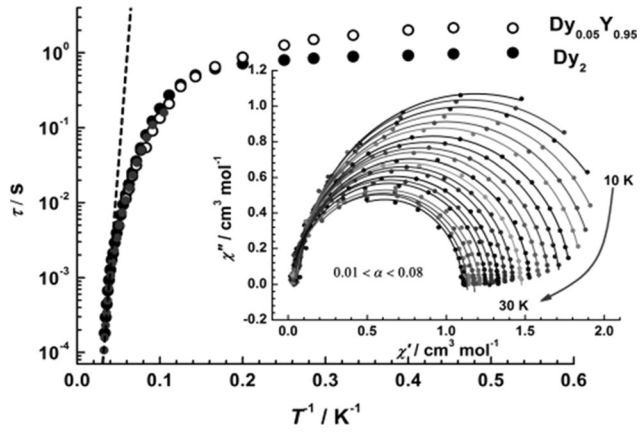

Figure 4. Magnetization relaxation time τ versus T^{-1} for pure (Dy_2) and diluted ($Dy_{0.05}Y_{0.95}$) samples. The dashed lines represent the best fits to the Arrhenius law of the thermally activated region with the parameters given in the text. Inset: Cole–Cole plots for **1** at zero field between 10 and 30 K. The solid lines are the best fits to the experiments with the generalized Debye model.

tems, nearly quadrupling the previous mark of 76 K observed for a phenoxido-linked Dy_2 compound.[14a] However, on further cooling, compound **1** crossed over into a pure quantum regime below 5 K with a τ_{QTM} value of 1 s. Cole–Cole plots of χ'' versus χ' (Figure 4, inset and Figure S9 of the Supporting Information) between 1.9 and 30 K showed an evolution from asymmetrical arcs to semicircular profiles and were fitted to a generalized Debye model.[28] The parameter $\alpha \leq 0.08$ in the thermally activated region also confirms the presence of a single relaxation mechanism. Due to the large thermal barrier and a considerably slower tunneling rate, we were able to observe an S-shaped hysteresis cycle with a large opening below 1 T at temperatures up to 5 K by using the sweep rates accessible with a conventional magnetometer on a polycrystalline sample (Figure 5 and Figure S10 of the Supporting Information). A small step at $H = 0.4$ T corresponds to an exchange-bias field associated with a spin flip of the antiferromagnetically coupled Dy^{III} spins.

To further probe the QTM effect, diluted samples of **1** were prepared in a Dy:Y molar ratios of 1:19 by cocrystallization with the isostructural Y_2 complex **1a**. As shown in Figure S11 (Supporting Information), at 1:19 dilution, no obvious shift of the χ'' signal occurs over the same temperature range (5–21 K) in comparison to the undiluted sample (Figure 3, bottom). This can be taken as an indication that thermally activated relaxation is of single-ion origin. However, in the low-temperature region (below 5 K), the peak begins to shift toward slower frequencies (<1 Hz), until at 1.9 K it reaches the frequency limit (0.04 Hz) of the measurement. As a result, the relaxation times at low temperatures are one order of magnitude slower than those operating in the undiluted sample. Variable-field magnetization data also display a significant opening below 1 T at temperatures up to 6 K with two apparent steps (Figure 5 and Figure S12 of the Supporting Information). The larger step corresponds to zero-field QTM of the DyY species, and the smaller step at 0.4 T is due to the exchange-bias interaction of the Dy_2 species.

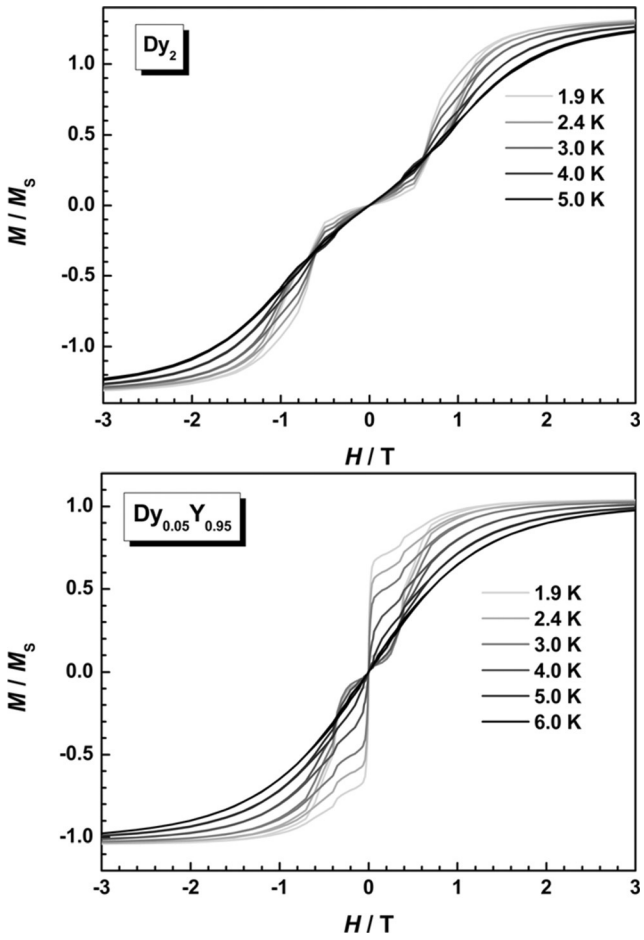

Figure 5. Plot of magnetization M versus field H for Dy_2 and $Dy_{0.05}Y_{0.95}$.

With the change in local coordination environment of Dy^{III} from N_2O_6 in **1** to O_8 in **2**, a strong divergence of dynamics behavior is observed. Compound **2** showed a slowly relaxing magnetic moment only at low temperatures (below 6 K) and no open $M(H)$ hysteresis loops (Figure S8 and Figure S13 of the Supporting Information). To probe the feasibility of lowering the relaxation probability via the quantum pathway, ac susceptibilities were measured under applied field. Indeed, as is commonly observed in lanthanide systems,[29] application of a field of 700 Oe has practically no effect on the dynamics of the thermally activated region but significantly slows down the relaxation rates in the temperature-independent regime compared with the situation under zero dc field (Figures S14 and S15 in the Supporting Information).The relaxation times extracted from $\chi''/\chi_{dc}(T)$ at 700 Oe exhibit an exponential dependence on temperature above 4 K, and an Arrhenius fit to the data gave an effective relaxation barrier of $U_{eff} = 34.8$ K and $\tau_0 = 2.0 \times 10^{-7}$ s.

Further insight into the electronic structure and magnetic blocking in the investigated dysprosium complexes was obtained by ab initio calculations. All calculations were performed with the MOLCAS program package[30] and were of CASSCF/RASSI/SINGLE_ANISO type[31] (Supporting Information, Tables S3–S7). This computational approach has been successful-

ly applied before for the investigation of lanthanide compounds.[4b,12,32] In particular, this computational methodology proved reliable in determination of the orientation of the local magnetic axes in the lowest electronic states of metal sites,[33] and quite recently it was shown to also give a trustworthy spectrum of the crystal-field splitting of the lowest *J* manifolds of lanthanide-based complexes.[34] Current ab initio methods are not suitable for treating several magnetic centers simultaneously; therefore, appropriate fragmentation was imposed. In the present calculations, Lu^{3+} was used in place of neighboring magnetic Dy^{3+}, and the positions of all other atoms of the studied complexes were kept as in the experimental X-ray structure. All atoms were described by ANO-RCC relativistic basis sets[35] available in the MOLCAS package.[30] Contractions of the employed basis sets are listed in Table S5 of the Supporting Information. The active space of the CASSCF method included nine electrons from the last shell spanning seven 4f orbitals of the Dy^{3+} ion. All spin states were optimized in state-average CASSCF calculations. Furthermore, all spin sextet, 128 spin quartet, and 130 spin doublet states were mixed by spin–orbit coupling in the RASSI program.[30,31] The resulting spin–orbital states were further used by SINGLE_ANISO for computation of local magnetic properties: *g* tensors for ground and excited states, main magnetic axes, local magnetic susceptibility, parameters of the crystal field for the ground atomic multiplet, and so on.

Further, the ab initio calculated low-lying spin–orbit states on individual Dy sites were employed in the phenomenological Lines model describing the exchange interaction between the Dy sites. Dipolar magnetic interaction was computed exactly and added to the Lines exchange matrix by using the ab initio results. Diagonalization of the total interaction matrix (exchange and dipolar) gives the spectrum of coupled eigenstates, which is further used as basis for description of the magnetism of the entire binuclear compounds. For these purposes we employed the POLY_ANISO program.[36]

As shown in Table 1, the energy spectrum of the states arising from the ground-state free-ion $J=15/2$ manifold differs drastically in the two compounds. The total splitting of the lowest manifold for **1** is almost twice that of **2**. Moreover, in **1** we found a large energy separation between the ground and first excited doublet, whereas in **2** nearly six Kramers doublets (KDs) lie within this energy range. Magnetic axialities of the ground-state doublets of **1** and **2** also differ strongly. The ground-state and first excited doublets of the Dy sites in **1** are highly axial, close to Ising anisotropy. Their corresponding main magnetic axes are almost collinear, with a small angle of 3.7° between them (Figure 6). In **2**, the ground-state doublet of the Dy sites displays large values of the transversal components of the *g* tensor ($g_{X,Y}$) (Table 1). These findings reveal the quite different crystal fields felt by Dy sites in the investigated compounds.

To rationalize the differences in the crystal field felt by the Dy^{3+} ion in **1** and **2**, we followed previously presented computational methodology of derivation of the parameters of the crystal field for the ground *J* manifold in lanthanide complexes from ab initio calculations.[34] Table S6 (Supporting Information) shows the ab initio derived crystal field for the investigated compounds. We note that, in the case of **1**, the dominant ligand-field effect comes from the axial O_2^0 parameter, whereas in the case of **2**, the dominant effect originates from the non-axial O_2^{-1} parameter. These data are in good agreement with the magnetization blocking in **1** (Figures 2 and 3) in zero dc field and absence of magnetization blocking in **2** under the same conditions.

Table 1. Ab initio calculated low-lying energy spectrum and magnetic anisotropy of the two lowest KDs on individual dysprosium sites of **1** and **2**.

KD	Dy_2 (**1**)	Dy_2Zn_2 (**2**)
1	0.0	0.0
2	219.6	14.9
3	318.8	33.6
4	360.9	58.2
5	432.7	119.0
6	474.1	142.0
7	504.8	256.8
8	549.7	278.1
	g tensors	
g_x[a]	1.5×10^{-3}	1.59
g_y[a]	2.0×10^{-3}	2.67
g_z[a]	19.73	15.20
g_x[b]	0.17	1.64
g_y[b]	0.24	6.20
g_z[b]	16.31	11.08

[a] KD 1. [b] KD 2.

The main magnetic axis of Dy sites in **1** form a small angle with the shortest chemical bond (Dy–O2) of 10.7° (Figure 6). The short Dy–O2 bond is a sign of the dominant covalent effect of the O2 atom in the ligand field of Dy. The electrostatic perturbation arising from O2 is also dominant in **1**. This is revealed by comparison of the LoProp atomic charges[37] of the first-sphere coordinated atoms around the magnetic lanthanide center by using the ground-state wave function. This analysis showed that O2 also bears the highest negative atomic charge (−0.896) among all atoms in the first coordination sphere of the Dy center. In fact, it is quite common that the main magnetic axis of strongly axial Dy compounds or fragments is oriented along the ligand atom that exerts the strongest perturbation (i.e., usually it is the closest ligand atom).

In **2**, the main magnetic axis of the ground KD of the Dy site forms a significantly larger angle with the closest ligand oxygen atom (O2). However, we note that the main anisotropy axis forms a small angle with the O1 oxygen atom (CIF label), which actually bears the largest negative charge (Supporting Information, Table S7) among all first-sphere coordinated ligand atoms. In this case, it seems that the effect of the closest oxygen atom is compensated (and even slightly surpassed) by the effect of the ligand with the larger negative charge. As a result, the ligand field acting on the central Dy center in **2** does not have a clear dominant perturbation arising from one ligand atom. Consequently, the magnetic axiality of the ground state of Dy site in **2** is significantly reduced compared to **1**.

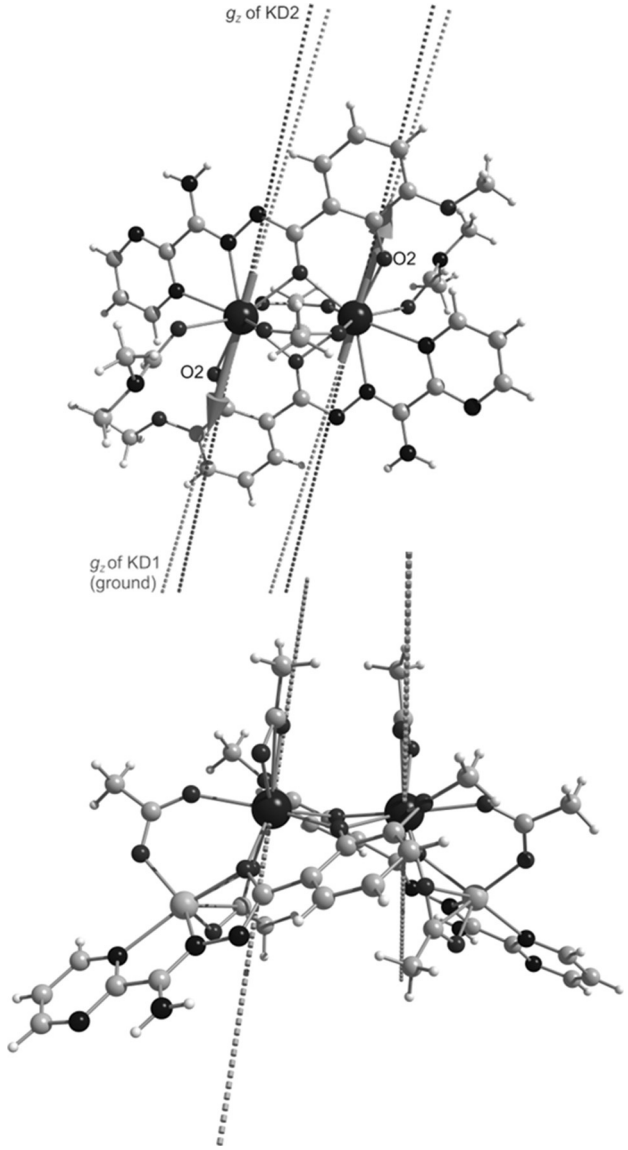

Figure 6. Orientations of the local magnetic moments in **1** (top) and **2** (bottom).

The results for individual metal sites obtained ab initio were further used for the computation of the exchange spectrum and magnetic properties of the binuclear complexes with the POLY_ANISO program.[36,38] The exchange interaction between Ln sites was considered within the Lines model,[39] whereas the contribution of the intramolecular dipole–dipole magnetic coupling was accounted for exactly, given that all necessary data were available from the ab initio calculations. Best-fit Lines parameters of the exchange interaction for the investigated compounds are listed in Table 2. On the basis of the resulting exchange spectrum of the entire system, all macroscopic magnetic properties were computed.

The magnetic interaction (exchange + dipolar) between the lowest KDs on sites can be calculated in good approximation by the noncollinear Ising Hamiltonian [Eq. (1)]

$$\hat{H}_{exch} = -J\hat{\tilde{S}}_{z1}\hat{\tilde{S}}_{z2} \qquad (1)$$

Table 2. Exchange and dipolar interactions [Eq. (1)] and the corresponding low-lying exchange spectra of **1** and **2** [cm^{-1}].

Interaction	1	2
dipolar[a]	−2.650	0.020
exchange	−8.375	−0.102
total	−11.025	−0.082
Doublet	Total low-lying spectrum of the binuclear compounds	
1	0.000	0.000
2	0.000	0.033
3	5.291	0.071
4	5.291	0.135
5	219.954	14.596
6	219.954	14.733
Doublet	g_z values in the two low-lying exchange doublet states[b]	
1	0.000	13.368
2	39.471	15.933

[a] Only the z_1z_2 term of the dipolar interaction is shown here. All terms were included in the POLY ANISO calculation. [b] $g_{x,y}=0$ for non-Kramers doublets, in view of the Griffith theorem.[40]

in which $J = J_{dipolar} + J_{exchange}$ is the parameter of total magnetic interaction between metal sites and $\hat{\tilde{s}}_{zi} = 1/2$ is the pseudospin of the ground doublet state of the corresponding Dy sites.

As already inferred from the measured magnetism, the S shape of the low-temperature low-field molar magnetization for **1** is a sign of strong antiferromagnetic coupling between metal sites. Indeed, a reasonable theoretical description of measured magnetic susceptibility and molar magnetization is achieved by quite large values of intramolecular magnetic interaction between Dy sites (Table 2). Notably, the exchange interaction is stronger than the dipolar magnetic coupling, and both of them act in the same direction, that is, towards stabilizing the nonmagnetic state (Table 2). In **2**, the perpendicular arrangement of the local magnetic axes with respect to each other and to the Dy–Dy axis does not favor strong dipolar magnetic interaction. Exchange interaction is also found to be significantly lower compared to **1**. The reason for this could lie in the structural differences of the bridging paths promoting the interaction. In **1** the two magnetic sites are 1) connected by four bridges and 2) the two Dy and two O1 atoms are coplanar. In **2** 1) only two bridges connect the Dy atoms, 2) the two Dy and two bridging O2 atoms are not coplanar (dihedral angle 159°), and 3) the distance between magnetic sites in **2** is larger than in **1**. Broken-symmetry DFT calculations on the Gd equivalents of **1** and **2** revealed much stronger antiferromagnetic exchange interaction in the former but an almost negligible value for the interaction in the latter (Supporting Information, Tables S8 and S9).

Conclusion

We have isolated excellent Dy_2 SMM **1** with fourfold connections derived from bis(μ_2-O) bridging groups and two acetate ligands in a *syn-syn* μ_2-η^1:η^1 mode. The incorporation of two Zn^{II} ions in the pockets on either side of the Dy_2O_2 core afforded complex **2**, in which only slow relaxation is observed. In view of the magnetostructural correlation, the occupation of the N_2O pocket by Zn^{II} in **2** breaks the strong axial anisotropy

and decreases the Dy···Dy coupling, which is reinforced through two straddling acetate groups in **1**. Ab initio calculations revealed more axial *g* tensors as well as first excited KDs that were highest in energy for **1**, corresponding to the higher energy barrier observed experimentally in **1**. Further insight into magnetic coupling indicated that the four bridging paths in **1** play an important role in promoting the dipolar and exchange interactions between Dy sites compared to other reported antiferromagnetic dinuclear lanthanide systems. The present results demonstrate that 1) for suitable crystal fields on the Dy sites, strong axiality of the local doublets produced from one significant chemical covalent bond leading to an efficient blocking of magnetization can be achieved and 2) it is a relatively simple way to enhance the magnetic interaction as opposed to the more synthetically challenging methods, such as the introduction of radical bridges or organometallic complexes. This work provides a proper model for understanding the synergic effect between single-ion anisotropy and magnetic interactions in augmenting the anisotropic barrier.

Experimental Section

General procedures

All chemicals were used as commercially obtained without further purification. Elemental analysis for carbon, hydrogen, and nitrogen was carried out with a PerkinElmer 2400 analyzer. FTIR spectra were recorded with a PerkinElmer FTIR spectrophotometer by using the reflectance technique (4000–300 cm^{-1}). Samples were prepared as KBr disks. All magnetization data were recorded on a Quantum Design MPMS-XL7 SQUID magnetometer. The variable-temperature magnetization was measured with an external magnetic field of 1000 Oe in the temperature range of 1.9–300 K. Samples were restrained in eicosane to prevent torquing. The experimental magnetic susceptibility data are corrected for the diamagnetism estimated from Pascal's tables[26] and sample holder calibration.

X-ray crystallography

Crystallographic data were collected at 191 K on a Bruker Apex II CCD diffractometer with graphite-monochromated $Mo_{K\alpha}$ radiation ($\lambda = 0.71073$ Å). Data were processed with the SAINT program. The structure was solved by direct methods and refined on F^2 by full-matrix least-squares techniques with SHELXTL97.[41] The location of Ln atom was easily determined, and O, N, and C atoms were subsequently located in the difference Fourier maps. The non-hydrogen atoms were refined anisotropically. The H atoms were introduced in calculated positions and refined with fixed geometry with respect to their carrier atoms. CCDC 1062931, 1062916, and 1062932 contain the supplementary crystallographic data for this paper. These data can be obtained free of charge from The Cambridge Crystallographic Data Centre.

Synthesis of 1, 1a, 2, and the diluted sample

$[Dy_2(a'povh)_2(OAc)_2(DMF)_2]$ (1): Solid $Dy(OAc)_3{\cdot}H_2O$ (0.2 mmol, 71.5 mg) was added to a slurry of H_2**a′povh** (28.7 mg, 0.1 mmol) and NaOH (0.016 mg, 0.4 mmol) in CH_3OH/DMF (10/2 mL). The mixture was stirred for a further 6 h and then filtered. Yellow block-shaped single crystals of **1**, suitable for X-ray diffraction analysis, formed after two weeks. Yield: 24 mg (28%, based on the metal salt); elemental analysis calcd (found) for $C_{36}H_{42}N_{12}O_{12}Dy_2$: C 37.28 (36.91), H 3.65 (3.52), N 14.49 (14.31); IR (KBr): $\tilde{\nu} = 3467$ (br), 3327 (br), 3069 (w), 2934 (w), 2828 (w), 1661 (w), 1635 (s), 1583 (s), 1562 (s), 1513 (s), 1468 (s), 1410 (s), 1385 (m), 1335 (m), 1264 (w), 1221 (m), 1191 (w), 1180 (w), 1070 (w), 1041 (w), 952 (w), 859 (w), 794 (w), 736 (w), 711 (w), 676 (w), 645 (w), 615 cm^{-1} (w).

$[Y_2(a'povh)_2(OAc)_2(DMF)_2]$ (1a): The preparation of this compound followed the same procedure as for **1** except that $Y(OAc)_3{\cdot}H_2O$ (0.2 mmol, 56.8 mg) was used as the starting material instead of $Dy(OAc)_3{\cdot}H_2O$. Yield: 32 mg (32%, based on the metal salt); elemental analysis calcd (found) for $C_{36}H_{42}N_{12}O_{12}Y_2$: C 42.70 (42.36), H 4.18 (4.13), N 16.60 (16.41); IR (KBr): $\tilde{\nu} = 3467$ (br), 3328 (br), 3069 (w), 2934 (w), 2829 (w), 1661 (w), 1635 (s), 1583 (s), 1562 (s), 1511 (s), 1468 (s), 1410 (s), 1385 (m), 1335 (m), 1264 (w), 1221 (m), 1191 (w), 1180 (w), 1070 (w), 1041 (w), 952 (w), 859 (w), 794 (w), 736 (w), 711 (w), 676 (w), 645 (w), 614 cm^{-1} (w).

$Dy_{0.05}Y_{0.95}$: The site-substituted $Dy_{0.05}Y_{0.95}$ sample was synthesized in accordance with the synthesis of pure **1** (see above), with an accurately measured 19:1 molar ratio of the yttrium(III) and dysprosium(III) acetate starting materials.

$[Zn_2Dy_2(a'povh)_2(OAc)_6]{\cdot}4H_2O$ (2): Solid $Dy(OAc)_3{\cdot}H_2O$ (0.2 mmol, 71.5 mg) and NaOH (0.016 mg, 0.4 mmol) were added to a solution of H_2**a′povh** (0.2 mmol, 54.2 mg) in CH_3OH/CH_2Cl_2 (10/10 mL). After stirring for 2 h, $Zn(OAc)_2{\cdot}2H_2O$ (43.9 mg, 0.2 mmol) was added to the resulting yellow solution. The mixture was stirred for a further 3 h and then filtered. Brown block-shaped single crystals of **2**, suitable for X-ray diffraction analysis, formed after 3 d. Yield: 35 mg (24%, based on the Dy^{III} salt); elemental analysis calcd (found) for $C_{38}H_{44}N_{10}O_{22}Zn_2Dy_2$: C 31.50 (31.41), H 3.06 (2.97), N 9.67 (9.60); IR (KBr): $\tilde{\nu} = 3466$ (br), 3332 (br), 3067 (w), 2940 (w), 2842 (w), 1668 (w), 1595 (s), 1571 (s), 1507 (s), 1414 (s), 1374 (m), 1326 (w), 1230 (m), 1196 (w), 1084 (w), 1049 (w), 959 (w), 843 (w), 807 (w), 746 (w), 711 (w), 682 (w), 660 (w), 618 cm^{-1} (w).

Acknowledgements

We thank the National Natural Science Foundation of China (Grants 21371166, 21301136, 21221061 and 21331003) for financial support. L.U. is a post-doc of the Fonds Wetenschappelijk Onderzoek-Vlaanderen, and also gratefully acknowledges INPAC and Methusalem grants of K.U. Leuven.

Keywords: dysprosium · ab initio calculations · magnetic properties · N,O ligands · single-molecule magnets

[1] F. Luis, A. Repollés, M. J. Martínez-Pérez, D. Aguilà, O. Roubeau, D. Zueco, P. J. Alonso, M. Evangelisti, A. Camón, J. Sesé, L. A. Barrios, G. Aromí, *Phys. Rev. Lett.* **2011**, *107*, 117203.

[2] M. Urdampilleta, S. Klyatskaya, J. P. Cleuziou, M. Ruben, W. Wernsdorfer, *Nat. Mater.* **2011**, *10*, 502.

[3] S. Thiele, F. Balestro, R. Ballou, S. Klyatskaya, M. Ruben, W. Wernsdorfer, *Science* **2014**, *344*, 1135.

[4] a) J. D. Rinehart, J. R. Long, *Chem. Sci.* **2011**, *2*, 2078; b) L. Ungur, J. J. Le Roy, I. Korobkov, M. Murugesu, L. F. Chibotaru, *Angew. Chem. Int. Ed.* **2014**, *53*, 4413; *Angew. Chem.* **2014**, *126*, 4502.

[5] a) P. Zhang, Y.-N. Guo, J. Tang, *Coord. Chem. Rev.* **2013**, *257*, 1728; b) J. Tang, P. Zhang, *Lanthanide Single Molecule Magnets*, Springer, Heidelberg, **2015**.

[6] J. D. Rinehart, M. Fang, W. J. Evans, J. R. Long, *J. Am. Chem. Soc.* **2011**, *133*, 14236.

[7] L. Ungur, S.-Y. Lin, J. Tang, L. F. Chibotaru, *Chem. Soc. Rev.* **2014**, *43*, 6894.
[8] N. Ishikawa, M. Sugita, T. Ishikawa, S.-y. Koshihara, Y. Kaizu, *J. Am. Chem. Soc.* **2003**, *125*, 8694.
[9] J. Tang, I. Hewitt, N. T. Madhu, G. Chastanet, W. Wernsdorfer, C. E. Anson, C. Benelli, R. Sessoli, A. K. Powell, *Angew. Chem. Int. Ed.* **2006**, *45*, 1729; *Angew. Chem.* **2006**, *118*, 1761.
[10] J.-L. Liu, Y.-C. Chen, Y.-Z. Zheng, W.-Q. Lin, L. Ungur, W. Wernsdorfer, L. F. Chibotaru, M.-L. Tong, *Chem. Sci.* **2013**, *4*, 3310.
[11] K. R. Meihaus, J. R. Long, *J. Am. Chem. Soc.* **2013**, *135*, 17952.
[12] L. Ungur, L. F. Chibotaru, *Phys. Chem. Chem. Phys.* **2011**, *13*, 20086.
[13] Y.-N. Guo, L. Ungur, G. E. Granroth, A. K. Powell, C. Wu, S. E. Nagler, J. Tang, L. F. Chibotaru, D. Cui, *Sci. Rep.* **2014**, *4*, 5471.
[14] a) J. R. M. Long, F. Habib, P.-H. Lin, I. Korobkov, G. Enright, L. Ungur, W. Wernsdorfer, L. F. Chibotaru, M. Murugesu, *J. Am. Chem. Soc.* **2011**, *133*, 5319; b) Y.-N. Guo, G.-F. Xu, W. Wernsdorfer, L. Ungur, Y. Guo, J. Tang, H.-J. Zhang, L. F. Chibotaru, A. K. Powell, *J. Am. Chem. Soc.* **2011**, *133*, 11948.
[15] R. J. Blagg, L. Ungur, F. Tuna, J. Speak, P. Comar, D. Collison, W. Wernsdorfer, E. J. L. McInnes, L. F. Chibotaru, R. E. P. Winpenny, *Nat. Chem.* **2013**, *5*, 673.
[16] J. D. Rinehart, M. Fang, W. J. Evans, J. R. Long, *Nat. Chem.* **2011**, *3*, 538.
[17] F. Tuna, C. A. Smith, M. Bodensteiner, L. Ungur, L. F. Chibotaru, E. J. L. McInnes, R. E. P. Winpenny, D. Collison, R. A. Layfield, *Angew. Chem. Int. Ed.* **2012**, *51*, 6976; *Angew. Chem.* **2012**, *124*, 7082.
[18] S. Demir, J. M. Zadrozny, M. Nippe, J. R. Long, *J. Am. Chem. Soc.* **2012**, *134*, 18546.
[19] P. H. Lin, T. J. Burchell, R. Clérac, M. Murugesu, *Angew. Chem. Int. Ed.* **2008**, *47*, 8848; *Angew. Chem.* **2008**, *120*, 8980.
[20] a) Y.-N. Guo, X.-H. Chen, S. Xue, J. Tang, *Inorg. Chem.* **2011**, *50*, 9705; b) P. Zhang, L. Zhang, S.-Y. Lin, S. Xue, J. Tang, *Inorg. Chem.* **2013**, *52*, 4587.
[21] F. Habib, G. Brunet, V. Vieru, I. Korobkov, L. F. Chibotaru, M. Murugesu, *J. Am. Chem. Soc.* **2013**, *135*, 13242.
[22] a) S. A. Sulway, R. A. Layfield, F. Tuna, W. Wernsdorfer, R. E. P. Winpenny, *Chem. Commun.* **2012**, *48*, 1508; b) Q. Zhou, F. Yang, D. Liu, Y. Peng, G. Li, Z. Shi, S. Feng, *Inorg. Chem.* **2012**, *51*, 7529.
[23] S. Xue, Y.-N. Guo, L. Zhao, P. Zhang, J. Tang, *Dalton Trans.* **2014**, *43*, 1564.
[24] S. Xue, Y.-N. Guo, P. Zhang, J. Tang, unpublished results.
[25] S. K. Langley, N. F. Chilton, B. Moubaraki, K. S. Murray, *Inorg. Chem.* **2013**, *52*, 7183.
[26] O. Kahn, *Molecular Magnetism*, Wiley-VCH, Weinheim, **1993**.
[27] a) P.-H. Guo, J.-L. Liu, Z.-M. Zhang, L. Ungur, L. F. Chibotaru, J.-D. Leng, F.-S. Guo, M.-L. Tong, *Inorg. Chem.* **2012**, *51*, 1233; b) I. J. Hewitt, J. Tang, N. T. Madhu, C. E. Anson, Y. Lan, J. Luzon, M. Etienne, R. Sessoli, A. K. Powell, *Angew. Chem. Int. Ed.* **2010**, *49*, 6352; *Angew. Chem.* **2010**, *122*, 6496; c) S.-Y. Lin, W. Wernsdorfer, L. Ungur, A. K. Powell, Y.-N. Guo, J. Tang, L. Zhao, L. F. Chibotaru, H.-J. Zhang, *Angew. Chem. Int. Ed.* **2012**, *51*, 12767; *Angew. Chem.* **2012**, *124*, 12939.
[28] a) K. S. Cole, R. H. Cole, *J. Chem. Phys.* **1941**, *9*, 341; b) S. M. J. Aubin, Z. Sun, L. Pardi, J. Krzystek, K. Folting, L.-C. Brunel, A. L. Rheingold, G. Christou, D. N. Hendrickson, *Inorg. Chem.* **1999**, *38*, 5329.
[29] S. D. Jiang, B. W. Wang, G. Su, Z. M. Wang, S. Gao, *Angew. Chem. Int. Ed.* **2010**, *49*, 7448; *Angew. Chem.* **2010**, *122*, 7610.
[30] F. Aquilante, L. De Vico, N. Ferré, G. Ghigo, P.-å. Malmqvist, P. Neogrády, T. B. Pedersen, M. Pitoňák, M. Reiher, B. O. Roos, L. Serrano-Andrés, M. Urban, V. Veryazov, R. Lindh, *J. Comput. Chem.* **2010**, *31*, 224.
[31] a) P. Å. Malmqvist, B. O. Roos, B. Schimmelpfennig, *Chem. Phys. Lett.* **2002**, *357*, 230; b) L. F. Chibotaru, L. Ungur, *J. Chem. Phys.* **2012**, *137*, 064112.
[32] L. F. Chibotaru, L. Ungur, C. Aronica, H. Elmoll, G. Pilet, D. Luneau, *J. Am. Chem. Soc.* **2008**, *130*, 12445.
[33] L. Ungur, W. V. d. Heuvel, L. F. Chibotaru, *New J. Chem.* **2009**, *33*, 1224.
[34] R. Marx, F. Moro, M. Dorfel, L. Ungur, M. Waters, S. D. Jiang, M. Orlita, J. Taylor, W. Frey, L. F. Chibotaru, J. van Slageren, *Chem. Sci.* **2014**, *5*, 3287.
[35] B. O. Roos, V. Veryazov, P.-O. Widmark, *Theor. Chem. Acc.* **2004**, *111*, 345.
[36] L. Ungur, M. Thewissen, J.-P. Costes, W. Wernsdorfer, L. F. Chibotaru, *Inorg. Chem.* **2013**, *52*, 6328.
[37] L. Gagliardi, R. Lindh, G. Karlström, *J. Chem. Phys.* **2004**, *121*, 4494.
[38] L. Ungur, L. F. Chibotaru, Computer programs SINGLE_ANISO and POLY_ANISO, KU Leuven.
[39] M. E. Lines, *J. Chem. Phys.* **1971**, *55*, 2977.
[40] J. S. Griffith, *Phys. Rev.* **1963**, *132*, 316.
[41] G. M. Sheldrick, *SHELXS-97 Program for Crystal Structure Solution*, University of Göttingen, Germany, **1997**.

Received: May 12, 2015
Published online on August 13, 2015